

# Electron surface layer at the interface of a plasma and a dielectric wall

R. L. Heinisch, F. X. Bronold, and H. Fehske

*Institut für Physik, Ernst-Moritz-Arndt-Universität Greifswald, 17489 Greifswald, Germany*

(Dated: November 28, 2018)

We study the potential and the charge distribution across the interface of a plasma and a dielectric wall. For this purpose, the charge bound to the wall is modelled as a quasi-stationary electron surface layer which satisfies Poisson's equation and minimizes the grand canonical potential of the wall-thermalized excess electrons constituting the wall charge. Based on an effective model for a graded interface taking into account the image potential and the offset of the conduction band to the potential just outside the dielectric, we specifically calculate the potential and the electron distribution for MgO, SiO<sub>2</sub> and Al<sub>2</sub>O<sub>3</sub> surfaces in contact with a helium discharge. Depending on the electron affinity of the surface, we find two vastly different behaviors. For negative electron affinity, electrons do not penetrate into the wall and an external surface charge is formed in the image potential, while for positive electron affinity, electrons penetrate into the wall and a space charge layer develops in the interior of the dielectric. We also investigate how the electron surface layer merges with the bulk of the dielectric.

PACS numbers: 52.40.Hf, 73.30.+y, 52.80.Tn

## I. INTRODUCTION

Macroscopic objects in contact with an ionized gas acquire a negative charge because the influx of electrons from the plasma outruns the influx of ions. The collection of electrons at the wall (boundary of the object) gives rise to a repulsive Coulomb potential which reduces the electron influx until the wall charge reaches a quasi-stationary value. As a consequence of the electron accumulation at the wall an electron depleted region, the plasma sheath, is formed adjacent to the wall.

Most of the voltage driving the discharge drops across the sheath. Wall charges may however not only affect the spatial structure of the plasma but also surface-supported elementary process such as electron-ion recombination and secondary electron emission, which are particularly important in dusty plasmas,<sup>1-3</sup> dielectric barrier discharges,<sup>4-6</sup> and solid-state based micro-discharges.<sup>7-11</sup> A macroscopic description of the wall charge, sufficient for the modeling of the plasma sheath,<sup>12</sup> is clearly insufficient for quantifying the effect wall charges might have on these processes. A microscopic description of the wall charge and the potential across the plasma-wall interface it leads to is required.

Traditionally, plasma walls are treated as perfect absorbers.<sup>12-14</sup> Irrespective of the microscopic interaction, all electrons and ions impinging on the wall are assumed to recombine instantly. From this model only the wall potential just outside the wall can be obtained. This is the potential that balances the electron and ion influx at the wall. A first, qualitative step going beyond this model was taken by Emeleus and Coulter,<sup>15,16</sup> who envisaged the wall charge as a two-dimensional surface plasma coupled to the bulk plasma via electron-ion wall recombination. No attempt was however made to put this appealing idea onto a formal basis. Later the notion of a two-dimensional surface charge was developed further by Behnke and coworkers<sup>17-19</sup> utilizing

phenomenological rate equations for the electron and ion surface densities. In these equations, the microphysics at the wall is encapsulated in surface parameters, such as, electron and ion sticking coefficients, electron and ion desorption times, and an electron-ion wall recombination coefficient. In principle these parameters can be calculated. Assuming, for instance, plasma electrons to ad- and desorb in the long-range image potential of the wall we calculated in our previous work electron sticking coefficients and electron desorption times for uncharged metallic<sup>20</sup> and dielectric surfaces.<sup>21-23</sup> We also made a first attempt to estimate these two quantities for charged dielectric plasma walls<sup>24</sup> and proposed a physisorption-inspired microscopic charging model for dust particles in a gas discharge.<sup>25</sup>

In this work, we will focus on a different issue and investigate the quasi-stationary potential and charge distribution across the interface of a plasma and a dielectric wall. For simplicity we will assume the perfect absorber model to be valid, that is, the wall potential simply balances at a certain distance from the crystallographic interface the electron and the ion influx from the plasma. In the model outlined below the quasi-stationary electron adsorbate bound to the wall is treated as an electron surface layer which is in thermal equilibrium with the wall. Its chemical potential, width, and position relative to the crystallographic interface depends on surface and plasma parameters. Our primary aim is to determine the electronic structure not only in front of the wall as it is done in models for the plasma sheath<sup>12-14</sup> but across the plasma-wall interface.

To calculate the modification of the charge distribution and the potential across the plasma-wall interface arising from the excess electrons of the wall charge, we use an effective one-dimensional model for a graded interface that encompasses the long-range image potential and the surface dipole of the bare surface responsible for the offset of the conduction band minimum to the poten-

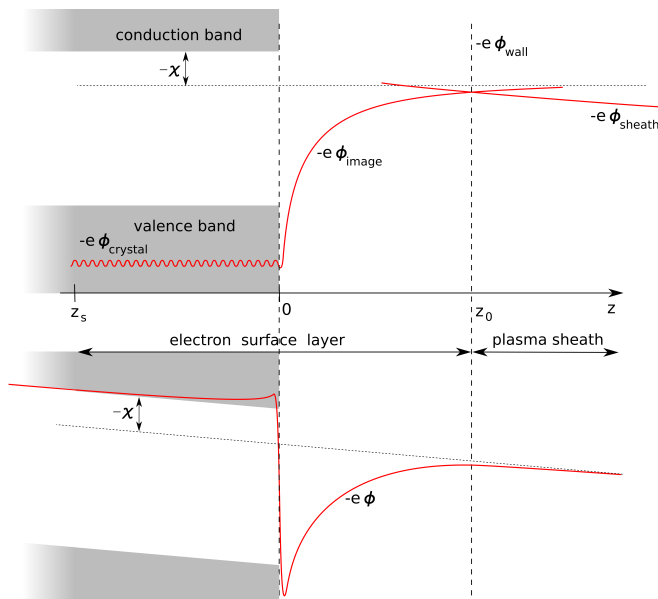


FIG. 1: Qualitative sketch of an interface between a plasma and a dielectric wall. Upper panel: Band structure, microscopic crystal potential merging with the image potential, and sheath potential. Lower panel: Effective potential for the graded interface on which our model of an electron surface layer is based.

tial just outside the dielectric. The model of a graded interface, originally proposed by Stern for the interface between two dielectrics,<sup>26</sup> and later on used by others for semiconductor heterojunctions<sup>27</sup> and electron trapping in nanopores,<sup>28</sup> guarantees continuity of the electrostatic potential across the plasma-wall interface. It thus allows us to study the spatial distribution of wall charges across the interface. To insert the wall charge into the interface we follow Tkharev and Danilyuk<sup>29</sup> and minimize, in the spirit of density functional theory<sup>30,31</sup>, the grand canonical potential of the wall-thermalized excess electrons. We also investigate how the electron surface layer merges with the bulk of the dielectric.

The remaining paper is structured as follows. In Sec. II we first construct a crude model for an electron surface layer at the interface between a plasma and a dielectric wall. It does not account for the merging of the electron surface layer with the bulk of the dielectric. As long as the primary interest is in the region close to the crystallographic interface and the band gap of the dielectric is large enough, the crude model is sufficient. Section III describes a refinement of the model which enables one to also investigate the cross-over of the electron surface layer to the bulk of the dielectric. This is particularly important for dielectrics with small energy gaps. Numerical results for the potential and the electron distribution are given in Section IV and a short summary is formulated in Sec. V.

## II. CRUDE ELECTRON SURFACE LAYER

As depicted in Fig. 1, we consider an ideal, planar interface at  $z = 0$  with the dielectric occupying the half-space  $z < 0$  and the discharge occupying the half-space  $z > 0$ . Chemical contamination and structural damage due to the burning gas discharge are discarded. At the moment we focus on the physical principles controlling the electronic properties of the plasma-wall interface. In the model we propose the wall charge to be treated as an electron surface layer (ESL) which is an interface specific electron distribution thermalized with the solid stretching from the plasma sheath over the crystallographic interface to the bulk of the dielectric.

The boundary between the ESL and the plasma sheath is located in front of the surface at  $z = z_0$ . It is the position where the attractive force due to the surface potential  $\phi_{surf}$  and the repulsive force due to the sheath potential  $\phi_{sheath}$  balance each other. Thus,  $z_0$  is given by

$$\phi'_{surf}(z_0) + \phi'_{sheath}(z_0) = 0. \quad (1)$$

It gives the position of an effective wall for plasma electrons and ions at which, for instance, the flux balance condition of the perfect absorber model,  $j_e = j_i$ , with  $j_e$  and  $j_i$ , respectively, the electron and ion flux towards the dielectric surface, has to be fulfilled. For  $z < z_0$  an electron is attracted to the surface and thus contained in the ESL while for  $z > z_0$  it is repelled back into the plasma. On the solid side, for  $z < 0$ , the ESL is bounded because of the shallow potential well formed by the restoring force from the positive charge in the plasma sheath.

In this section we will outline the essential building blocks of the ESL model. Putting together concepts from plasma as well as surface physics a detailed, self-contained account seems to be helpful.

### A. Plasma sheath

In the traditional view, electrons missing in the positive space charge region in front of the plasma wall accumulate on the wall and give rise to a wall potential. For the construction of our one-dimensional interface model we need the total number per unit area of missing sheath electrons (that is, the total surface density of missing sheath electrons) as a function of the wall potential because it is this number of electrons which can be distributed across the ESL. Hence, we require a model for the plasma sheath.

For simplicity, we use a collisionless sheath<sup>12</sup>, more realistic sheath models<sup>12-14</sup> make no difference in principle. In the collisionless sheath electrons are thermalized, that is, the electron density  $n_e = n_0 \exp(e\phi/k_B T_e)$ , with  $\phi$  the potential,  $n_0$  the plasma density and  $T_e$  the electron temperature. The ions enter the sheath with a directed velocity  $v_{i0}$  and satisfy a source-free continuity equation,

$d(n_i v_i)/dz = 0$ , implying  $n_i v_i = n_0 v_{i0}$ , and an equation of motion  $M(v_i \frac{d}{dz} v_i) = -e \frac{d}{dz} \phi$ , with  $n_i$  the ion density, and  $M$  the ion mass. The potential  $\phi$  satisfies Poisson's equation  $d^2 \phi / dz^2 = -4\pi e(n_i - n_e)$ . Thus, the governing equations for the collisionless plasma sheath are<sup>12</sup>

$$v_i \frac{dv_i}{dz} = -\frac{e}{M} \frac{d\phi}{dz} \quad \text{and} \quad (2)$$

$$\frac{d^2}{dz^2} \phi = -4\pi e n_0 \left[ \frac{v_0}{v_i} - \exp\left(\frac{e\phi}{k_B T_e}\right) \right]. \quad (3)$$

Using dimensionless variables

$$\eta = -\frac{e\phi}{k_B T_e}, \quad \xi = \frac{z}{\lambda_D}, \quad \text{and} \quad u = \frac{v_i}{c_s} \quad (4)$$

where

$$\lambda_D = \sqrt{\frac{k_B T_e}{4\pi n_0 e^2}} \quad \text{and} \quad c_s = \sqrt{\frac{k_B T_e}{M}} \quad (5)$$

equations (2) and (3) become

$$uu' = \eta' \quad \text{and} \quad (6)$$

$$\eta'' = \frac{u_0}{u} - \exp(-\eta). \quad (7)$$

In the ESL model the plasma occupies not the whole half space  $z > 0$  but only the portion  $z > z_0$  (see Fig. 1). Hence, the integration of the first equation gives  $u = -\sqrt{2\eta + u_0^2}$ , where  $u_0 = v_{i0}/c_s$  is the reduced velocity of ions entering the sheath, so that the second equation becomes

$$\eta'' = -\frac{u_0}{\sqrt{2\eta + u_0^2}} - \exp(-\eta). \quad (8)$$

Using the boundary condition that the potential and the field vanish far inside the plasma, that is,  $\eta \rightarrow 0$  and  $\eta' \rightarrow 0$  for  $\xi \rightarrow \infty$ , Eq. (8) can be integrated once and we obtain

$$\eta' = -\sqrt{-2u_0 \sqrt{2\eta + u_0^2} + 2 \exp(-\eta) + 2u_0 \sqrt{u_0^2} - 2}. \quad (9)$$

For ions entering the sheath with the Bohm velocity  $u_0 = -1$ . The field at the wall as a function of the wall potential  $\eta_w = \eta(\xi_0)$  is then given by

$$\eta'_w = -\sqrt{2\sqrt{2\eta_w + 1} + 2 \exp(-\eta_w) - 4}. \quad (10)$$

The total surface density of electrons in the ESL equals the total surface density of missing sheath electrons, in other words, the total surplus surface density of positive ions in the sheath  $N$  which can be calculated from the electric field at the wall. Integrating Poisson's equation yields

$$\begin{aligned} N &= \int_{z_0}^{\infty} dz (n_i - n_e) = -\frac{1}{4\pi e} \int_{z_0}^{\infty} dz \frac{d^2 \phi}{dz^2} \\ &= \frac{1}{4\pi e} \frac{d\phi}{dz}(z_0) = -n_0 \lambda_D \eta'_w. \end{aligned} \quad (11)$$

Combing Eqs. (11) and (10) gives the total surface density of electrons to be inserted into the ESL as a function of the wall potential.

The wall potential itself is determined by the flux balance condition,  $j_e = j_i$ , which, in the ESL model, is assumed to be fulfilled at  $z = z_0$ . Using the Bohm flux for the ions and the thermal flux for the electrons,

$$j_i = n_0 \sqrt{\frac{k_B T_e}{M}} \quad \text{and} \quad j_e = \frac{1}{4} n_0 \sqrt{\frac{8k_B T}{\pi m_e}} e^{\frac{e\phi}{k_B T_e}}, \quad (12)$$

the wall potential is given by

$$\eta_w = \frac{1}{2} \ln \left( \frac{M}{2\pi m_e} \right), \quad (13)$$

that is,

$$\phi_w = -\frac{k_B T_e}{2e} \ln \left( \frac{M}{2\pi m_e} \right). \quad (14)$$

In the collisionless sheath model the wall potential depends only on the electron temperature and the ion to electron mass ratio.

## B. Surface dipole

We now turn to the interface region in which the missing sheath electrons will be inserted. This region is absent in the traditional modeling of plasma walls. In our model it is an extended region surrounding an ideal dielectric surface. In comparison to the electrons responsible for the chemical binding within the dielectric the additional electrons coming from the plasma are only a few. The electronic structure of the surface, for instance, the available electronic states and the offset of the energy bands in the bulk with respect to the potential outside the dielectric will thus not be changed significantly by the presence of the wall charge.

In order to quantify the above statement let us first consider the electrostatic potential and the electronic structure of a free-standing dielectric surface. According to Tung,<sup>32</sup> it has to minimize the thermodynamical potential and satisfy Poisson's equation implying that the potential is continuous across the surface. Strictly speaking, the continuity of the potential only applies to the microscopic crystal potential which has to merge continuously with the surface potential outside the crystal. The averaged long-range potential, in contrast, can be discontinuous at the interface.

The energy of an electronic state in the bulk of the dielectric can be referenced to the vacuum level  $V(\infty) = 0$ , that is, the potential far outside the crystal, in the following way,<sup>32</sup>

$$E_{ik}(\vec{r}) = \epsilon_{ik} - e\bar{V}_{cell} - eV_s(\vec{r}), \quad (15)$$

where  $\epsilon_{ik}$  is the quantum-mechanical contribution to the energy,  $\bar{V}_{cell}$  is averaged potential of a cell due to the

charge distribution within the same cell, and  $V_s(\vec{r})$  is the long range potential due to the surface dipole, space charges, and external fields. In the simple two-band model depicted in Fig. 1,  $i = v, c$ .  $V_s(\vec{r})$  is composed of a slowly varying component due to external fields and space charges as well as the surface dipole responsible for the potential offset at the surface. The plasma effect due to external fields and space charges will be accounted for by Poisson's equation (see below). In order to judge whether the plasma affects the surface dipole it is useful to consider first the typical strength of the surface dipole of a free-standing dielectric surface.

The surface dipole included in  $V_s(\vec{r})$  results from a charge double-layer in immediate proximity to the surface. Depending on the material it can have various origins. For an ionic crystal, for example, due to lattice relaxation at the surface, anions or cations can protrude while the other species is retracted (e.g. protruding oxygen and retracted cations for magnesium oxide<sup>33</sup>) and, more importantly, as a result of the minimization of the thermodynamic potential, the electron density leaks out into the vacuum. As a result a charge double-layer is formed over a length on the order of a lattice constant. The dipole layer is usually characterized by a dipole strength

$$eD = eV_s(\vec{r}_s^-) - eV(\vec{r}_s^+), \quad (16)$$

where  $V_s(\vec{r}_s^-)$  is the limit of the long range potential just inside the crystal at the surface position  $\vec{r}_s$  and  $V(\vec{r}_s^+)$  is the limit of the potential at that position just outside the surface. Usually these two potentials are termed the potential just inside and the potential just outside, respectively.<sup>32,34</sup> Here, just outside denotes a distance small compared to variations of the long-range potential due to external fields or space charges but large compared with the width of the charge double-layer. Note that in the definition of the potential just outside the image potential is assumed to have already decreased to zero. This will be important later.

The strength of the dipole layer is a microscopic property of the surface which is relatively insensitive against the additional charges from the plasma. The reason for this lies in the small number of additional electrons from the plasma compared to the number of displaced electrons involved in the formation of the dipole layer. To prove this statement we give a simple estimate. Typical surface dipoles  $eD$  are on the order of electron Volts. For a double-layer of one  $\text{\AA}$  to each side of the crystallographic interface a potential difference of one Volt requires a surface charge density of  $5.5 \times 10^{13} \text{cm}^{-2}$ . The surface charge density at the wall of a helium discharge with plasma density  $n_0 = 10^7 \text{cm}^{-3}$  and electron temperature  $k_B T_e = 2eV$  amounts, however, only to  $4.4 \times 10^6 \text{cm}^{-2}$ . For typical plasma densities, the number of additional electrons is thus far too small to lead to a change of the surface dipole. Even for semiconductor-based microdischarges<sup>8,10</sup>, which can have much higher plasma densities, we expect the surface dipole of the

plasma wall not to be modified by the plasma.

In view of the just given estimate, we have to revise an assumption in our previous work,<sup>23</sup> where we assumed the surface charge accumulating on the wall would increase the dipole energy  $eD$  by  $e\phi_w$ , leading to the image states being pushed from the band gap into the energy region of the conduction band. The numbers given in the previous paragraph indicate, however, that the band line-up of the conduction band and the potential just outside the solid, will not be affected much by the wall charge. Hence, if a negative electron affinity supports image states in front of the uncharged surface, these states remain in the band gap for the charged surface. Electron trapping as investigated in Refs.<sup>21,22</sup> is thus even possible for charged plasma walls.

Instead of the dipole strength  $eD$  which cannot be measured directly, it is more convenient to characterize the dipole layer by the electron affinity  $\chi$  which is a measurable quantity for a dielectric surface.<sup>34</sup> The electron affinity is the energy released when an electron is moved from just outside the surface to the bottom of the conduction band.

From Eq. (15) it is clear that  $\chi$  equals  $eD$  plus a bulk contribution,

$$\chi = -eV_s(\vec{r}_s^+) - E_{ck}(\vec{r}_s^-) = eD - E_C + e\bar{V}_{cell}, \quad (17)$$

where  $E_C = \epsilon_{cm}$  denotes the minimum of the conduction band. We can thus use  $\chi$  to characterize the potential offset at the surface. There is however a caveat. The long-range potential inside the solid is only specified up to a constant.<sup>32</sup> Typical choices are the cell-averaged potential or the inter-sphere potential of the muffin-tin approximation. For our purpose it will be however more convenient to take the conduction band minimum as the long-range potential inside the solid. This choice is motivated as follows. We are considering a dielectric with a large energy gap. The valence band is thus fully occupied and the conduction band is essentially empty. Hence, only the conduction band can be populated by additional electrons coming from the plasma and referencing the electrostatic potential inside the solid to the conduction band minimum allows us to relate the total surplus electron density in the interface region to the potential in the interface region in analogy to what we have done for the plasma sheath in the previous subsection.

Adopting the above discussion to the one-dimensional model shown in Fig. 1 and assuming a quadratic dispersion for the conduction band, the energy of an electron in the conduction band is given by

$$E_k(z) = \frac{\hbar^2 k^2}{2m_c^*} - e\phi_{surf}(z), \quad (18)$$

where  $\phi_{surf}(z)$  is the total surface potential to be determined in the next subsection and the offset of the electrostatic potential at the surface,

$$e\phi_{surf}(0^-) - e\phi_{surf}(0^+) = \chi, \quad (19)$$

encompasses the surface dipole as well as the unspecified bulk contribution.

### C. Image potential

The surface potential of the bare surface comprises the surface dipole and a long-range contribution, the image potential, resulting from the mismatch of the dielectric constants at the surface. Far away from the surface the image potential is given by<sup>35</sup>

$$\phi_{im}(z) = \frac{\epsilon - 1}{4(\epsilon + 1)} \frac{e}{z}. \quad (20)$$

But this expression cannot be employed for our purpose because the singularity at  $z = 0$  prohibits a smooth electron distribution across the interface. In reality the image potential has to continuously merge with the crystal potential. Equation (20) is thus also unphysical.

To obtain a realistic surface potential without performing an atomistically accurate calculation we employ the model of a graded interface. Initially proposed by Stern<sup>26</sup> to remove the unphysical singularity of the image potential at the interface of two dielectrics, the model assumes the dielectric constant  $\epsilon$  to vary over a distance on the order of a lattice constant. Later the graded interface model was extended to variations of other physical quantities and applied to semiconductor heterostructures and nanopores.<sup>27,28</sup>

In the spirit of a graded interface, we assume the dielectric constant  $\epsilon$ , the electron mass  $m$ , and the potential offset at the surface to vary smoothly according to the grading function

$$g_{c^-,c^+}(z) = \begin{cases} c^- & z < -a \\ \frac{c^- + c^+}{2} - \frac{c^- - c^+}{2} \sin\left(\frac{\pi x}{2a}\right) & -a < z < a \\ c^+ & z > a \end{cases}, \quad (21)$$

where  $a$  is the half width of the graded interface and  $c^\mp$  stands for the quantity that varies across the interface. We use the value  $a = 5\text{\AA}$  which is an estimate used in previous applications of the graded interface.<sup>26-28</sup> While the grading parameter  $a$  is not based on definite experimental or theoretical results it is motivated by the assumption that the bonding and the electron density at the surface change over one to two lattice constants implying a transition layer for the effective potential and the dielectric constant that is somewhat larger. Hence, across the interface the electron mass, the dielectric constant and the offset potential are given by

$$m(z) = g_{m_C^*, m_e}(z), \quad \epsilon(z) = g_{\epsilon, 1}(z), \quad (22)$$

and

$$\phi_{offset}(z) = \frac{1}{e} g_{\chi, 0}(z), \quad (23)$$

respectively, with  $m_C^*$  the effective mass of the conduction band.

Within the model of the graded interface, the image potential is the change in the selfenergy of an electron due to the proximity of the dielectric mismatch. Positioning the electron at  $\vec{r}_0$  it is given by<sup>26</sup>

$$\phi_{im}(\vec{r}_0) = \frac{1}{2} [\phi^m(\vec{r}_0) - \phi^0(\vec{r}_0)], \quad (24)$$

where  $\phi^m(\vec{r})$  is the potential in the medium with dielectric mismatch arising from the electron at  $\vec{r}_0$  and  $\phi^0(\vec{r})$  is the same quantity in a homogeneous medium with dielectric constant  $\epsilon(z_0)$ . Hence,  $\phi^m(\vec{r})$  is the solution of

$$\nabla(\epsilon(z)\nabla\phi^m(\vec{r})) = 4\pi e\delta(\vec{r} - \vec{r}_0) \quad (25)$$

while  $\phi^0(\vec{r})$  is the solution of

$$\nabla^2\phi^0(\vec{r}) = \frac{4\pi e}{\epsilon(z_0)}\delta(\vec{r} - \vec{r}_0). \quad (26)$$

To solve Eqs. (25) and (26) we follow Stern<sup>26</sup> and make the ansatz

$$\phi^{m,0}(z, \rho, \phi) = \frac{1}{2\pi} \sum_{l=-\infty}^{\infty} \int_0^{\infty} dq q J_l(\rho q) J_l(\rho_0 q) \times e^{il(\phi - \phi_0)} A_q^{m,0}(z). \quad (27)$$

Placing the electron on the  $z$  axis,  $\rho_0 = 0$  which implies  $J_0(\rho_0 q) = 1$  and  $J_l(\rho_0 q) = 0$  for  $l > 0$ . Hence, we need to keep only the  $l = 0$  term, so that

$$\phi^{m,0}(z, \rho, \phi) = \frac{1}{2\pi} \int_0^{\infty} dq q J_0(\rho q) A_q^{m,0}(z), \quad (28)$$

where  $A_q^0(z)$  is given by

$$A_q^0(z) = \frac{-2\pi e}{\epsilon(z_0)q} e^{-q|z - z_0|} \quad (29)$$

and  $A_q^m(z)$  is the solution of

$$A_q^{m''}(z) + \frac{\epsilon'(z)}{\epsilon(z)} A_q^{m'}(z) - q^2 A_q^m(z) = \frac{4\pi e}{\epsilon(z)} \delta(z - z_0) \quad (30)$$

which has to be obtained numerically. The image potential is then given by

$$\phi_{im}(z_0) = \frac{1}{4\pi} \int_0^{\infty} dq q (A_q^m(z_0) - A_q^0(z_0)). \quad (31)$$

In contrast to Eq. (20) it is now smoothly varying across the interface with a deep well on the low- $\epsilon$  side and a small bump on the high- $\epsilon$  side.

The total surface potential comprises the graded offset potential (23) and the graded image potential. Hence,

$$\phi_{surf}(z) = \phi_{im}(z) + \phi_{offset}(z). \quad (32)$$

It is continuous across the crystallographic interface at  $z = 0$  and enables us thereby to also calculate a smoothly varying electron distribution in the ESL. The band structure and the total surface potential at the graded interface are visualized in the lower panel of Fig. 1.

Using Eq. (1) we can now determine the position  $z_0$  of the effective wall, that is, the maximum extent of the ESL on the plasma side. The derivative of the bare surface potential is  $\phi'_{surf} = \phi'_{offset} + \phi'_{im}$ . Due to the relatively weak field in the sheath compared to the image force, the boundary  $z_0$  will be so far away from the interface that  $\phi'_{offset}$  vanishes and the image potential obeys (20). Thus, the boundary between the ESL and the plasma sheath is given by

$$z_0 = \sqrt{\frac{(\epsilon - 1)e}{4(\epsilon + 1)\phi'_w}} \quad (33)$$

with  $\phi'_w = -(k_B T_e \eta'_w)/(e\lambda_D)$  and  $\eta'_w$  given by (10).

#### D. Electron distribution

The wall charge is assumed to be in thermal equilibrium with the wall. Hence, the distribution of the excess electrons in the ESL has to minimize the excess electron's grand canonical potential in the external potential due to the surface. The coupling to the sheath is maintained by the constraint that only as many electrons can be filled into the ESL as are missing in the sheath and the boundary conditions to the Poisson equation which links the electron distribution in the ESL to the (internal) electrostatic potential.

To minimize the grand canonical potential we follow Tkharev and Danilyuk<sup>29</sup> and apply density functional theory<sup>30,31</sup> to the graded interface. Quite generally, the grand canonical potential of an electron system in an external potential  $V(\vec{r})$  is given in the local approximation by

$$\Omega = \int V(\vec{r})n(\vec{r})d\vec{r} + \frac{1}{2} \int \frac{e^2 n(\vec{r})n(\vec{r}')}{|\vec{r} - \vec{r}'|} d\vec{r}d\vec{r}' + G[n] - \mu \int n(\vec{r})d\vec{r}, \quad (34)$$

where  $G[n]$  is the grand canonical potential of the homogeneous system with density  $n(\vec{r})$ . The ground state electron density minimizes  $\Omega$ , that is, it satisfies

$$V(\vec{r}) + \int \frac{e^2 n(\vec{r}')}{|\vec{r} - \vec{r}'|} d\vec{r}' + \mu^h(n) - \mu = 0, \quad (35)$$

where  $\mu^h(n) = \delta G[n]/\delta n$  is the chemical potential for the homogeneous system.

Specifically for the excess electrons in the one-dimensional graded interface Eq. (35) reduces to

$$-e\phi(z) + \mu^h(z) - \mu = 0, \quad (36)$$

where  $\mu^h(z) \equiv \mu^h(n(z), T)$  and the electrostatic potential,

$$\phi(z) = \phi_{surf}(z) + \phi_C(z), \quad (37)$$

consists of the potential of the bare surface given by Eq. (19) and the internal Coulomb potential which satisfies Poisson's equation,

$$\frac{d}{dz} \left( \epsilon(z) \frac{d}{dz} \phi_C(z) \right) = 4\pi e n(z), \quad (38)$$

with the graded dielectric constant  $\epsilon(z)$  given by Eq. (22) and the boundary conditions  $\phi_C(z_0) = \phi_w$  and  $\phi'_C(z_0) = \phi'_w$  to guarantee continuity of the potential at  $z_0$  and to include the restoring force from the positive charge in the sheath.

For the functional relation  $\mu^h(z) \equiv \mu^h(n(z), T)$  we take the expression adequate for a homogeneous, non-interacting, non-degenerate electron gas,

$$n(z) = \frac{1}{\sqrt{2}} \left( \frac{m(z)kT}{\pi\hbar^2} \right)^{\frac{3}{2}} e^{\frac{\mu^h(z)}{k_B T}}. \quad (39)$$

This is justified because the density of the excess electrons is rather low and the temperature of the surface is rather high, typically a few hundred Kelvins.

In order to calculate the quasi-stationary electron distribution, Eqs. (36) and (38) have to be solved self-consistently with the additional constraint that the total electron surface density in the ESL equals the total surface density of electrons missing in the sheath, that is,

$$\int_{z_s}^{z_0} dz n(z) = N, \quad (40)$$

with  $N$  given by Eq. (11). In the above equation we introduced a cut-off  $z_s < 0$  at which the ESL terminates inside the dielectric. As long as  $|z_s|$  is chosen large enough it does not affect the numerical results close to the surface. An improved treatment of the ESL, avoiding the ad-hoc cut-off, is given in the next section.

Within the crude ESL model developed in this section the computation is performed iteratively in the interval  $z_s < z < z_0$  according to the following scheme: (i) We start with the potential of the empty surface given by Eq. (37) with  $\phi_C(z)$  obtained from Eq. (38) with  $n(z) = 0$  but with the boundary conditions at  $z_0$  as specified. (ii) We integrate both sides of Eq. (39) over  $z$  with  $\mu^h(z)$  given by Eq. (36). Enforcing the constraint (40) determines  $\mu$ . (iii) Using  $\mu$  we calculate from Eq. (36) a new  $\mu^h(z)$  which gives with Eq. (39) a new electron density  $n(z)$ . (iv) Lastly, we determine from Eq. (38) the electrostatic potential associated with the up-dated  $n(z)$ . Steps (ii) - (iv) are iterated until  $\mu$ , which is far below the conduction band edge because of the non-degeneracy of the excess electrons, converges.

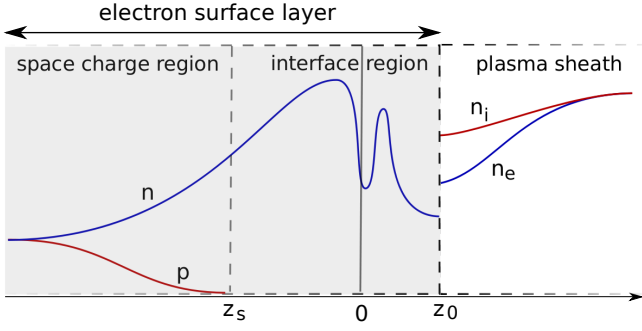


FIG. 2: Sketch of the refined model of the interface between a plasma and a dielectric wall. In the plasma equal densities of electrons and ions ensure quasi-neutrality. The positive space charge in front of the effective wall defines the plasma sheath. The ESL contains a very narrow interface-specific region (ISR) where the model of the graded interface is used and a wide space charge region (SCR) which allows a continuous merging with the neutral bulk of the dielectric where intrinsic electrons and holes balance each other to guarantee charge neutrality. Note, the widths of the various regions are not to scale.

### III. REFINED ELECTRON SURFACE LAYER

In the previous section we have taken into account only the electron concentration in the conduction band of the dielectric due to the electrons coming from the plasma. For wide band gap materials this is justified, especially near the surface, as their concentration is much larger than the intrinsic carrier concentration. Deep inside the dielectric, however, charge neutrality is not enabled by a vanishing electron density, but by the electron density decreasing to its intrinsic value, which is then balanced by the intrinsic hole concentration in the valence band.

To take this effect into account, which is particularly important when the additional electrons accumulate deep inside the bulk of the dielectric, we divide the ESL into two regions: a very narrow interface-specific region (ISR) and a wide space charge region (SCR) in the bulk of the dielectric. The parameter  $z_s$  denotes now no longer an ad-hoc cut-off but the boundary between the two regions. It has to be chosen so that the ISR includes the major effect of the image potential in the dielectric implying  $z_s < -z_0$ . The electron distribution and the potential in the ISR are calculated using the density functional approach outlined in the previous section. In the SCR we use for simplicity the model of an intrinsic semiconductor to describe electron and hole densities as well as the long-range potential. As the energy bands in the dielectric follow the long-range potential the refined ESL also captures the band bending which might be induced by the presence of the wall charge. It is however only significant when most of the excess electrons are trapped in the SCR and not in the ISR.

Figure 2 schematically shows the electron and hole densities for the refined ESL model. The boundary between the plasma sheath and the ESL is still located at  $z_0$ . As

our model does not encompass the electron and ion flux from the plasma for  $z < z_0$ , the densities  $n_e$  and  $n_i$  are discontinuous at  $z_0$ . This is obvious for the ions which are not allowed to enter the solid. The discontinuity of the electron density, in contrast, arises because we ensure only the total number of missing sheath electrons per unit area to be conserved. This global constrained cannot guarantee continuity of the electron density at  $z_0$ . At the boundary between the ISR ( $z_s < z < z_0$ ) and the SCR ( $z < z_s$ ) the electron density and the potential are continuous. In principle, also the hole density  $p$  should be continuous. As  $p(z_s) \ll n(z_s)$  for the materials we are considering, we can however neglect holes in the ISR.

For the modeling of the SCR it is convenient to use  $\psi(z) = \phi(z) - \phi_{\text{bulk}}$  for the long range potential, which vanishes for charge neutrality in the bulk. Here,  $\phi_{\text{bulk}} = \phi(-\infty)$  (see below for an explicit relation for  $\phi_{\text{bulk}}$ ). Then, Poisson's equation is given by,

$$\frac{d^2\psi(z)}{dz^2} = -\frac{4\pi}{\epsilon} (-en(z) + ep(z)) , \quad (41)$$

where the electron and hole densities for an intrinsic semiconductor with parabolic bands whose extremal points are, respectively,  $E_C$  and  $E_V$  are given by<sup>36</sup>

$$n(z) = \frac{1}{\sqrt{2}} \left( \frac{m_C^* k_B T}{\pi \hbar^2} \right)^{\frac{3}{2}} e^{\frac{1}{k_B T} (\nu - E_C + e\psi(z))} , \quad (42)$$

$$p(z) = \frac{1}{\sqrt{2}} \left( \frac{m_V^* k_B T}{\pi \hbar^2} \right)^{\frac{3}{2}} e^{-\frac{1}{k_B T} (\nu - E_V + e\psi(z))} . \quad (43)$$

From a comparison of the exponents in Eq. (42) and Eq. (39), where  $\mu_h$  is given by Eq. (36) we find

$$\nu = \mu + E_C + e\phi_{\text{bulk}} . \quad (44)$$

Far from the surface,  $\psi = 0$  and  $n = p = n_b$ . This gives the chemical potential

$$\nu = \frac{E_V + E_C}{2} + \frac{3}{4} k_B T \ln \left( \frac{m_V^*}{m_C^*} \right) \quad (45)$$

and the bulk carrier concentration  $n_b$

$$n_b = \frac{1}{\sqrt{2}} \left( \frac{k_B T}{\pi \hbar^2} \right)^{\frac{3}{2}} (m_C^* m_V^*)^{\frac{3}{4}} \exp \left( -\frac{E_g}{2k_B T} \right) , \quad (46)$$

where  $E_g = E_C - E_V$ . Hence, Poisson's equation becomes

$$\frac{d^2\psi(z)}{dz^2} = \frac{4\pi e}{\epsilon} n_b \left( e^{\frac{e\psi(z)}{k_B T}} - e^{-\frac{e\psi(z)}{k_B T}} \right) \quad (47)$$

and using dimensionless variables

$$\eta = \frac{e\psi}{k_B T} \quad \text{and} \quad \xi = \frac{z - z_s}{L_D} \quad (48)$$

with  $L_D = \sqrt{\epsilon k_B T / 4\pi e^2 n_b}$  we obtain

$$\eta'' = e^\eta - e^{-\eta} . \quad (49)$$

This equation can be integrated once, which gives

$$(\eta')^2 = 4 \cosh(\eta) + C. \quad (50)$$

The boundary conditions in the bulk  $\eta = 0$  and  $\eta' = 0$  for  $\xi \rightarrow -\infty$  imply  $C = -4$  so that Eq. (50) becomes

$$\eta' = \sqrt{8} \sinh\left(\frac{\eta}{2}\right). \quad (51)$$

Integration with the boundary condition at  $z_s$ , that is, at  $\xi = 0$ ,  $\eta(0) = \eta_s$  and requiring  $\eta \rightarrow 0$  for  $\xi \rightarrow -\infty$  gives

$$\eta^\pm(\xi) = \mp 2 \ln \left[ \pm \tanh \left( \frac{\mp \xi}{\sqrt{2}} + \frac{c^\pm}{2} \right) \right] \quad (52)$$

with

$$c^\pm = \pm 2 \operatorname{artanh} \left[ \exp \left( \frac{\mp \eta_s}{2} \right) \right], \quad (53)$$

where the upper sign is for  $\eta_s > 0$  and the lower sign for  $\eta_s < 0$ .

In analogy to what we have done at the boundary of the ESL with the plasma sheath at  $z = z_0$  we relate the potential  $\eta_s$  to the total electron surface density in the space charge region. From Poisson's equation we obtain for the total electron surface density in the SCR

$$N^{SCR} = \int_{-\infty}^{z_s} dz (n - p) = L_D^2 n_b \left. \frac{d\eta}{dz} \right|_{-\infty}^{z_s} = L_D n_b \eta'(0), \quad (54)$$

where  $\eta'$  is given by Eq. (51), so that

$$N^{SCR} = \sqrt{8} L_D n_b \sinh\left(\frac{\eta_s}{2}\right), \quad (55)$$

or,

$$\eta_s = 2 \operatorname{arsinh} \left( \frac{N^{SCR}}{\sqrt{8} L_D n_b} \right). \quad (56)$$

For a negative space charge  $\eta_s > 0$ , so that the potential is given by  $\psi(z) = (k_B T/e) \eta^+((z - z_s)/L_D)$  and the electron and hole densities are given by  $n(z) = n_b e^{\eta^+((z - z_s)/L_D)}$  and  $p(z) = n_b e^{-\eta^+((z - z_s)/L_D)}$ , respectively. The relation between  $\psi$  and  $\phi$  is given by  $\phi_{bulk} = \phi(z) - \psi(z)$ . Since  $\psi(z_s) = (kT/e)\eta_s$  we obtain  $\phi_{bulk} = \phi(z_s) - (kT/e)\eta_s$ .

Now, quite generally, the electrons in the ESL are distributed over the ISR and SCR according to

$$N = N^{ISR}(\mu) + N^{SCR}(\mu), \quad (57)$$

where  $N^{ISR}$  is the surface density of electrons in the ISR,  $\mu$  is the chemical potential in both regions, and  $N$  is the total surface density of missing sheath electrons given by Eq. (11). The total surface density in the ISR is given by  $N^{ISR} = \int_{z_s}^{z_0} dz n(z)$ , where  $n(z)$  is calculated with

the density functional approach for the graded interface. Requiring continuity of the electron density at  $z_s$ ,

$$\frac{1}{\sqrt{2}} \left( \frac{m_C^* k_B T}{\pi \hbar^2} \right)^{\frac{3}{2}} e^{\frac{1}{k_B T}(\mu + e\phi(z_s))} = n_b e^{\eta_s}, \quad (58)$$

gives  $\eta_s$  as a function of  $\mu$ . From  $\eta_s$  we finally obtain using Eq. (55)  $N^{SCR}(\mu)$ .

For the calculation of the electron distribution and the potential in the refined ESL we use the iteration cycle described in the last section with one modification. In step (ii) we solve Eq. (57) instead of Eq. (40) to fix  $\mu$ . From  $\mu$  we obtain using Eq. (58)  $\eta_s$  which in turn determines the electron distribution and the potential in the SCR. This gives for each iteration step a continuous potential and electron distribution at  $z_s$ . As before, the steps (ii)-(iv) are iterated until  $\mu$  converges.

At the end of this section let us finally mention two simplifications of the refined ESL model which could be used, respectively, for large band gap dielectrics irrespective of the electron affinity and dielectrics with small band gap with positive electron affinity. In the former case the intrinsic carrier concentration  $n_b$  is very low and the merger with the bulk occurs very deep in the dielectric. Almost all surplus electrons are however much closer to the surface where the holes can be neglected. This can be seen from the differential equation for  $\eta$ . For small  $n_b$  Eq. (56) gives a large  $\eta_s$ . As  $\eta$  satisfies a highly nonlinear differential equation (49), a large  $\eta_s$  implies a steeper gradient of  $\eta$  near the surface so that almost all electrons are concentrated close to the surface where neglecting the holes has little effect. Hence, for large band gap dielectrics surplus electrons can be filled into a sufficiently large ISR for which the crude ESL model of the previous section will be sufficient provided the cut-off  $z_s$  is large enough. The merger with the bulk is of course not correctly captured by such an approach.

For dielectrics or semiconductors with small energy gaps and positive electron affinity, on the other hand, almost all surplus electrons are deep inside the material. It is thus a good approximation to neglect the ISR and to fill all electrons in a SCR. Neglecting the surface potential has little effect in this case and using the SCR already for  $z \leq 0$  gives a good description of the electron distribution inside the ESL. The electron density and potential at the surface and in front of it can of course not be captured by such an approach. As before  $\psi(z) = \phi(z) - \phi_{bulk}$  with  $\phi_{bulk} = \phi(z_s) - (k_B T/e)\eta_s$  where  $\phi(z_s)$  is now the limit of the long range potential just inside the dielectric given by  $\phi(z_s) = \phi_w + \chi/e$ .

#### IV. RESULTS

We now use the ESL model to calculate for a helium discharge in contact with a MgO, Al<sub>2</sub>O<sub>3</sub>, and SiO<sub>2</sub> surface the electron density and potential across the plasma wall. Our main focus lies in the identification of generic



TABLE I: Material parameters for some dielectrics. CB and VB stand for conduction and valence band, respectively.

	MgO	Al <sub>2</sub> O <sub>3</sub>	SiO <sub>2</sub>	GaAs
Dielectric constant $\epsilon_s$	9.8	9.9	3.78	13.1
Electron affinity $\chi$ [eV]	-0.4	2.5	1.3	4.07
CB effective mass $m_C^*$ [ $m_e$ ]	0.4	0.4	0.5	0.067
VB effective mass $m_V^*$ [ $m_e$ ]		4.0	0.58	0.45
Band gap $E_g$ [eV]		8.8	9.2	1.42

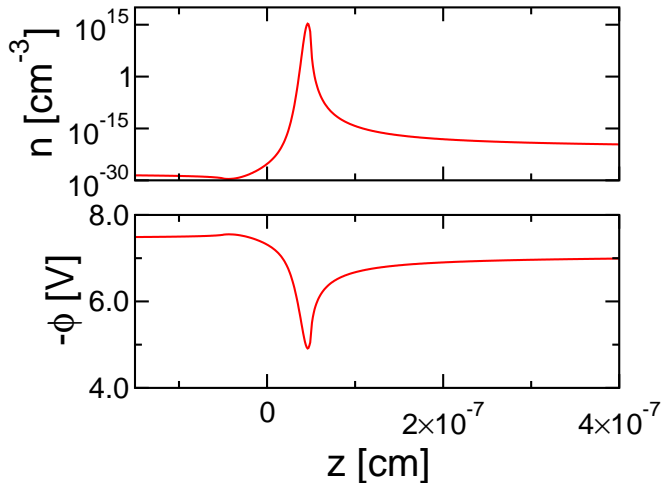


FIG. 3: Electron density  $n$  (upper panel) and potential  $-\phi$  (lower panel) at a MgO surface in contact with a helium discharge with  $n_0 = 10^7 \text{ cm}^{-3}$  and  $k_B T_e = 2 \text{ eV}$  calculated without accounting for a SCR in the dielectric (crude ESL model). The cut-off of the interface region is  $z_s = -z_0$ . As can be seen, almost all of the wall charge is located in the well of the image potential in front of the surface.

types of electron distributions in the ESL depending on plasma and surface parameters. Unless otherwise stated, we use for the plasma density  $n_0 = 10^7 \text{ cm}^{-3}$  and for the electron temperature  $k_B T_e = 2 \text{ eV}$ . The parameters of the dielectric surfaces are given in Table I.

First we give typical values for  $z_0$ , the position where the ESL merges with the plasma sheath. It is calculated from Eq. (1) and should thus depend not only on plasma but also on surface parameters. Our results for MgO ( $z_0 = 6.08 \times 10^{-5} \text{ cm}$ ), Al<sub>2</sub>O<sub>3</sub> ( $z_0 = 6.09 \times 10^{-5} \text{ cm}$ ), and SiO<sub>2</sub> ( $z_0 = 5.14 \times 10^{-5} \text{ cm}$ ) indicate however that  $z_0$  is relatively insensitive to  $\epsilon$ . Even the significantly smaller  $\epsilon$  of SiO<sub>2</sub> does not alter  $z_0$  considerably. For the helium discharge considered  $z_0$  is irrespective of the dielectric always on the order of a micron.

Of particular importance for the distribution of the electrons in the ESL is the electron affinity  $\chi$ , characterizing the offset of the conduction band to the potential just outside. For  $\chi < 0$  (MgO) the conduction band minimum lies above the potential just outside. It is thus energetically favorable for electrons to be located in the image potential in front of the surface. Figure 3 showing

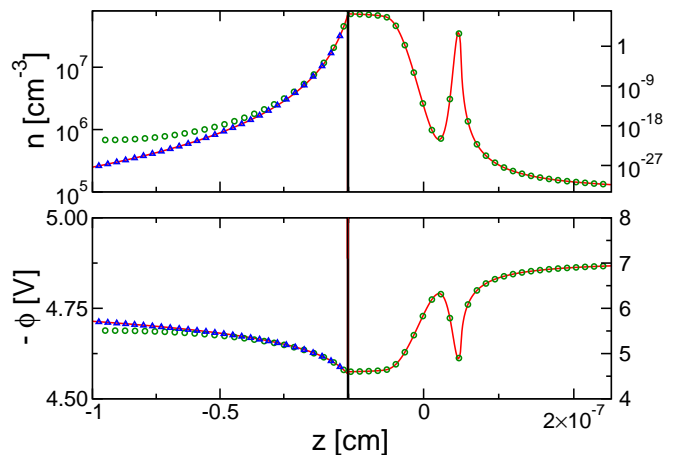


FIG. 4: Electron density  $n$  (upper panel) and potential  $-\phi$  (lower panel) at an Al<sub>2</sub>O<sub>3</sub> surface in contact with a helium discharge with  $n_0 = 10^7 \text{ cm}^{-3}$  and  $k_B T_e = 2 \text{ eV}$ . The red lines show data obtained from the refined ESL model accounting for an ISR and a SCR, the boundary between the two was put at  $z_s = -3z_0$ , the green circles show data for a model which consists only of an ISR with cut-off  $z_s = -0.9 \text{ cm}$  (crude ESL model), and the blue triangles show data for a model consisting only of a SCR for  $z < 0$ . Irrespective of the approximation, the wall charge extends deep into the bulk. Note the different scales of the axes for the left and right panels. On the spatial scale of the SCR shown in the left panels the ISR of the right panels becomes a vertical line.

the electron density and the potential in the ESL of MgO verifies this. The energy of an electron in the image potential  $-e\phi$  indeed reaches a minimum just in front of the surface at the beginning of the graded interface. For negative electron affinity, the excess electrons coming from the plasma thus form an external surface charge in the image potential in front of the crystallographic interface. The band bending associated with it is negligible.

For  $\chi > 0$ , on the other hand, the conduction band minimum is below the potential just outside. It is thus energetically favorable for electrons to accumulate inside the dielectric. This can be seen in Fig. 4 which shows the electron density and the potential in the refined (red line) and simplified ESL (open green circles and blue triangles) for an Al<sub>2</sub>O<sub>3</sub> surface. The surface potential consists of an attractive well in front of the surface but the minimum potential energy for electrons  $-e\phi$  is reached inside the dielectric. Excess electrons coming from the plasma are thus mostly located inside the wall and the electron distribution extends deep into the bulk. This extended negative space charge also leads to a band bending near the surface. Note the different scales of the axes for the left and right panels of Fig. 4. On the scale where variations in the SCR are noticeable the ISR is basically a vertical line.

If one neglects the SCR and fills all excess electrons into the ISR (crude ESL) the potential and the electron distribution are correctly described at and close to the surface but not far inside the dielectric (open green cir-

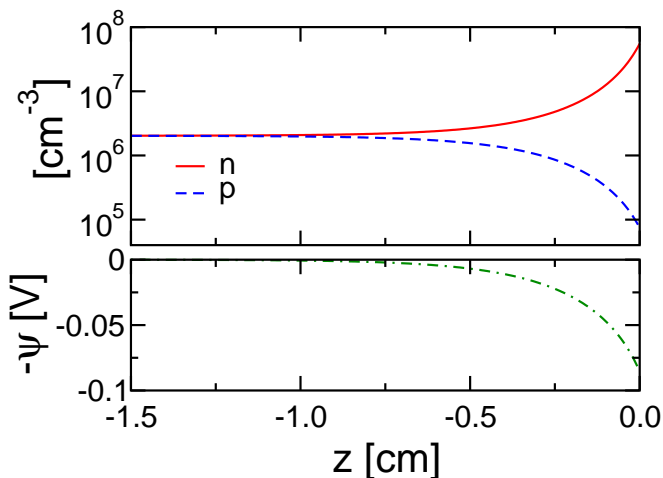


FIG. 5: Electron density  $n$  and hole density  $p$  at a GaAs surface in contact with a helium discharge with  $n_0 = 10^7 \text{ cm}^{-3}$  and  $k_B T_e = 2 \text{ eV}$  calculated with the refined ESL model without ISR. The wall charge sits inside the GaAs wall. Deep inside the bulk charge neutrality is achieved by an equal density of electrons and holes.

cles) because the ad-hoc cut-off  $z_s$  of the crude ESL leads to an unphysical pile-up of electrons near  $z_s$ . Hence, only if  $z_s$  is large enough does the crude ESL model give reliable results for the electron density and potential in the vicinity of the surface. Filling all electrons in the SCR, on the other hand, cannot describe the immediate vicinity of the surface correctly which is however on the scale of the SCR an infinitesimally narrow region. It gives only for  $z < -z_0$  a good description, that is, in the region where for  $\chi > 0$  indeed most of the electrons are located (blue triangles).

While the crude ESL model containing only an ISR gives the correct electron density near the surface provided  $z_s$  is large enough, the merger of the ESL with the bulk can only be described with the refined ESL model including the SCR. This is particularly relevant for materials with smaller band gaps and larger intrinsic carrier concentrations than MgO,  $\text{Al}_2\text{O}_3$ , and  $\text{SiO}_2$ . To exemplify this we show in Fig. 5 the electron and hole densities (upper panel) as well as the potential  $-\psi$  (lower panel) for a GaAs plasma wall, calculated for an ESL containing only a SCR. At the surface the electron density is about three orders in magnitude larger than the hole concentration. Deep inside the material electron and hole concentrations are equal, leading to charge neutrality and a constant potential. The band bending due to the extended space charge in the ESL is about  $0.09 \text{ eV}$ .

Our results for the electron and hole densities and the potential in the dielectric depend of course on the model for the SCR. We have used for simplicity the model of an intrinsic semiconductor which is appropriate for an undoped semiconductor without impurities. Depending on doping or impurities a variety of models<sup>37</sup> could be used to take material specific aspects into account. In

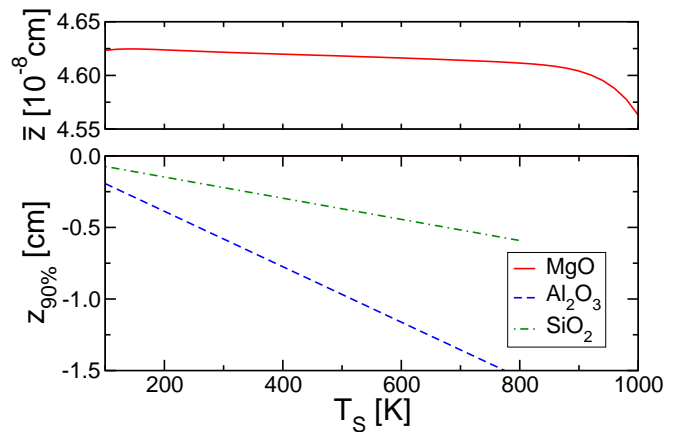


FIG. 6: Center of gravity  $\bar{z}$  of the electron distribution at a MgO surface (upper panel) and the  $z_{90\%}$  value for the electron distribution at an  $\text{Al}_2\text{O}_3$  and a  $\text{SiO}_2$  surface (lower panel), all in contact with a helium discharge with  $n_0 = 10^7 \text{ cm}^{-3}$  and  $k_B T_e = 2 \text{ eV}$ , as a function of the surface temperature  $T_s$ . The data shown in the upper and lower panel were obtained, respectively, from the crude ESL model and the refined ESL model without an ISR.

our exploratory calculation we obtain a rather wide SCR. Including the effect of impurities, acting as trapping sites in the band gap, would probably reduce the depth of the SCR considerably.

To summarize our results up to this point, we find that for negative electron affinity the electronic surface charge is located in front of the surface, while for positive electron affinity the electrons form a space-charge layer in the dielectric leading to a small bending of the energy bands.

The two distinct types of charge distributions in the ESL are also reflected in the dependence of the width of the electron distribution on the surface temperature. Figure 6 shows the center of gravity  $\bar{z}$  of the electron distribution for the MgO surface ( $\chi < 0$ ) and the  $z_{90\%}$  value for the surfaces of  $\text{Al}_2\text{O}_3$  and  $\text{SiO}_2$  ( $\chi > 0$ ), where  $z_{90\%}$  is implicitly defined by

$$\int_{z_{90\%}}^0 dz(n(z) - p(z)) = 0.9N. \quad (59)$$

We use the  $z_{90\%}$  value because it captures the depth of the SCR better than  $\bar{z}$  which depends too strongly on the few electrons that penetrate very deep into the bulk.

For negative electron affinity (MgO, shown in the upper panel of Fig. 6) the external surface charge is strongly trapped in the deep image potential so that  $\bar{z}$  changes very little with surface temperature. The width of the internal surface charge for dielectrics with positive electron affinity ( $\text{Al}_2\text{O}_3$  and  $\text{SiO}_2$ , lower panel), however, increases dramatically with surface temperature. This can be understood as follows. The restoring force from the positive ions in the sheath binds internal surface charges

only weakly to the surface. With increasing surface temperature, however, high-lying states in the conduction band get more and more populated. Hence, some electrons have rather high kinetic energies, are thus less confined near the surface by the weak restoring force, and penetrate therefore deeper into the bulk. As a result, the  $z_{90\%}$  value decreases strongly with surface temperature.

Let us now turn to the discussion of the influence of the electron temperature  $k_B T_e$  and the plasma density  $n_0$  on the properties of the ESL. These two parameters enter through the total surface density of electrons  $N$  depleting the sheath and accumulating in the ESL. How  $k_B T_e$  and  $n_0$  affect the interface depends therefore on the sheath model and the model used for the interaction between plasma particles and the surface. For simplicity we have used a collisionless sheath model and assumed the surface to be a perfect absorber for plasma electrons and ions. The results for the properties of the ESL as a function of the plasma parameters are thus to be taken only indicative.

The effect of a variation of  $n_0$  and  $k_B T_e$  is most significant for surfaces with positive electron affinity. Table II shows the effect of the plasma density  $n_0$  for a  $\text{SiO}_2$  surface. If  $n_0$  increases, the boundary  $z_0$  between sheath and ESL moves closer to the surface. This, however, does not affect the charge distribution much as most of the electrons occupy the SCR inside the dielectric (as shown in Fig. 4 for  $\text{Al}_2\text{O}_3$ ). More important is that an increase in  $n_0$  leads to an increase of the total surface electron density  $N$ . This entails a stronger restoring force from the plasma sheath so that the potential well confining the space charge inside the dielectric becomes steeper and the electrons in the SCR of the ESL are shifted towards the surface, in other words, the  $z_{90\%}$  value decreases with  $n_0$ . Mathematically, the steep-like shape of the electron distribution arises because a larger  $N$  leads through Eq. (56) to a larger  $\eta_s$  which makes the potential steeper at the surface so that the electron distribution is more peaked there. This trend can be seen in the lower panel for Fig. 7.

A variation of the electron temperature  $k_B T_e$  has similar effects as the variation of the plasma density. If  $k_B T_e$  increases, the total surface density of electrons increases also, as can be seen from Table III. As shown in the upper panel of Fig. 7, this leads again to a steep-like

TABLE II: Surface density of electrons in the ESL  $N$ , wall potential  $\phi_W$ , plasma sheath - ESL boundary  $z_0$  and the  $z_{90\%}$  value for  $\text{SiO}_2$  in contact with a helium discharge with  $k_B T_e = 2\text{eV}$  for different values of the plasma density  $n_0$ .

$n_0$ [ $10^6 \text{cm}^{-3}$ ]	$N$ [ $10^6 \text{cm}^{-2}$ ]	$\phi_W$ [V]	$z_0$ [ $10^{-5} \text{cm}$ ]	$z_{90\%}$ [cm]
10	4.38	-7.07	5.14	-0.222
20	6.20	-7.07	4.32	-0.157
50	9.80	-7.07	3.44	-0.099
100	13.9	-7.07	2.89	-0.070

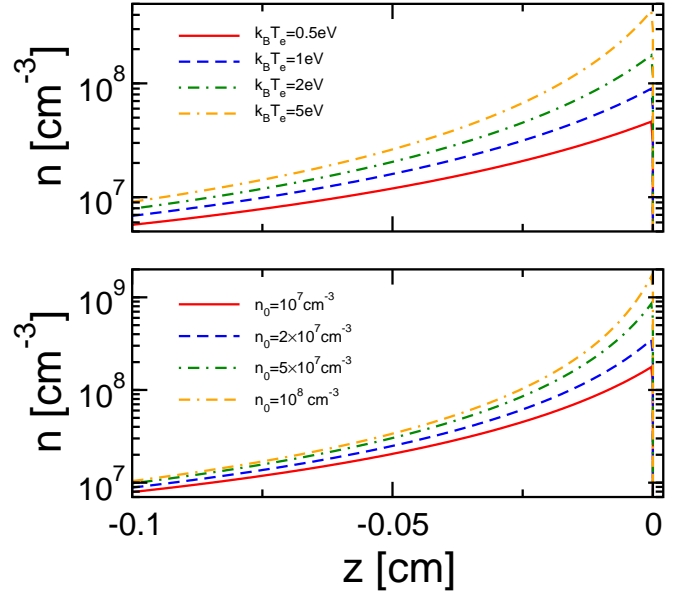


FIG. 7: Electron density  $n$  at a  $\text{SiO}_2$  surface in contact with a helium discharge as a function of the electron temperature (upper panel,  $n_0 = 10^7 \text{cm}^{-3}$ ) and the plasma density (lower panel,  $k_B T_e = 2\text{eV}$ ) for  $T_S = 300\text{K}$ . The refined ESL model without an ISR was employed to produce the data.

electron distribution which is the more concentrated at the surface the higher the electron temperature is.

For a surface with negative electron affinity ( $\text{MgO}$ ) the surplus electrons are strongly bound in the image potential. While a variation of  $k_B T_e$  or  $n_0$  changes the total number of surplus electrons per unit area in the same way as for a surface with positive electron affinity, the distribution of the surplus electrons within the ESL is not affected significantly because of the strong image interaction.

So far we have shown the potential and the electron distribution in the ESL. Now, we will compare potential and charge distribution in the ESL with the ones in the plasma sheath. The electron distribution at the interface is the quasi-stationary electron gas that guarantees flux equality at the sheath-ESL boundary  $z_0$ . As already mentioned not included in this simple model is the flux of plasma electrons and ions in the ESL before the electrons

TABLE III: Surface density of electrons in the ESL  $N$ , wall potential  $\phi_W$ , plasma sheath - ESL boundary  $z_0$  and the  $z_{90\%}$  value for  $\text{SiO}_2$  in contact with a helium discharge at  $n_0 = 10^7 \text{cm}^{-3}$  for different values of the electron temperature  $k_B T_e$ .

$k_B T_e$ [eV]	$N$ [ $10^6 \text{cm}^{-2}$ ]	$\phi_W$ [V]	$z_0$ [ $10^{-5} \text{cm}$ ]	$z_{90\%}$ [cm]
0.5	2.19	-1.77	7.27	-0.444
1	3.10	-3.53	6.11	-0.314
2	4.38	-7.07	5.14	-0.222
5	6.93	-17.7	4.086	-0.140

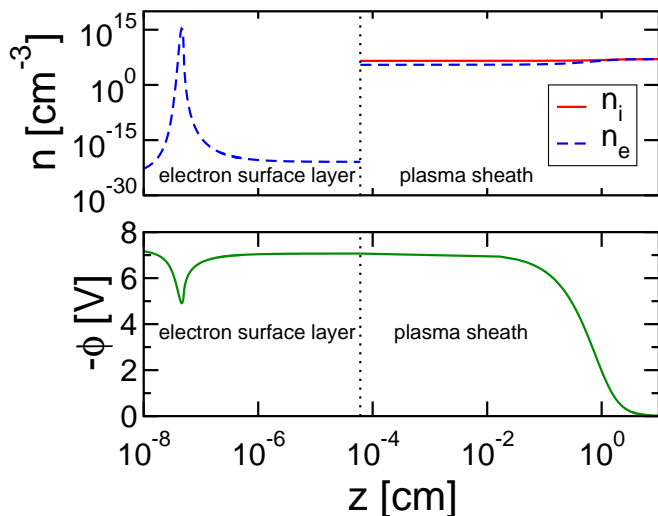


FIG. 8: Density of electrons trapped in the ESL as well as electron and ion density in the plasma sheath (upper panel) and potential (lower panel) for a MgO surface in contact with a helium discharge ( $n_0 = 10^7 \text{ cm}^{-3}$  and  $k_B T_e = 2 \text{ eV}$ ). The data were obtained from the crude ESL model.

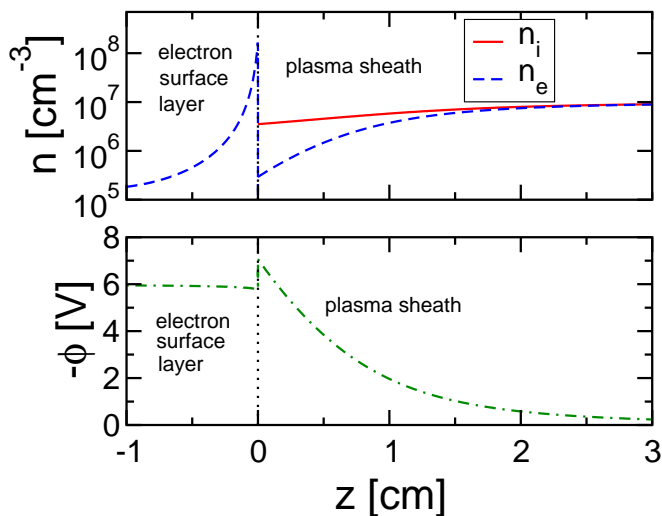


FIG. 9: Density of electrons in the ESL as well as electron and ion density in the plasma sheath (upper panel) and potential (lower panel) for a  $\text{SiO}_2$  surface in contact with a helium discharge ( $n_0 = 10^7 \text{ cm}^{-3}$  and  $k_B T_e = 2 \text{ eV}$ ). The refined ESL model without an ISR was employed to produce the data.

are trapped at the surface and the ions recombine with the negative wall charge. The electron and ion densities in this model are thus discontinuous at  $z_0$ . The potential, however, which has been obtained from the integration of Poisson's equation is continuous and differentiable everywhere. Between the well of the image potential and  $z_0$  the electron and ion flux from the sheath would be important. The neglect of the charge densities associated with these fluxes does however not affect the potential because they are too small to have a significant effect.

Figure 8 shows the ESL and the plasma sheath in front

of a MgO surface. Due to the negative electron affinity, the surface electrons are bound by the image potential in front of the surface. In Fig. 8, we plot the electron and ion density (upper panel), as well as the electric potential (lower panel) over the distance from the surface  $z$ . Far from the surface, the potential approaches the bulk plasma value chosen to be zero. In the sheath the potential develops a Coulomb barrier and reaches the wall potential  $\phi_w$  at  $z_0$ , the distance where the sheath merges with the surface layer (vertical dotted line). The wall potential is the potential just outside to which the energies of the bulk states are referenced. Closer to the surface the potential follows the attractive image potential while at the surface the repulsive potential due to the negative electron affinity prevents the electron from entering the dielectric (only scarcely seen on the scale of the figure).

In Fig. 9 we finally plot the electron and ion densities (upper panel) as well as the electric potential (lower panel) for  $\text{SiO}_2$ . Note the linear  $z$ -axis in contrast to the logarithmic  $z$ -axis of Fig. 8. Due to the positive electron affinity, the excess electrons constituting the wall charge penetrate deep into the dielectric and occupy therefore the SCR of the ESL. Compared to the variation of the electric potential in the sheath the band bending in the dielectric induced by the wall charge is rather small as indicated by the variation of  $\phi$  inside the dielectric. This is because  $\epsilon$  is large and the width of the SCR is narrow on the scale of the sheath. Only on the scale of the ISR (a vertical line at  $z = 0$ ) the SCR of the ESL is wide.

## V. CONCLUSIONS

We have studied the potential and the charge distribution across the interface of a plasma and a dielectric wall treating the wall charge as a quasi-stationary electron gas in thermal equilibrium with the dielectric. Our approach is based on a model for a graded bare surface including the offset between the potential just outside the dielectric and the conduction band minimum as well as the image potential due to the dielectric mismatch at the boundary. The missing electrons from the sheath populate the interface potential and thereby form an electron surface layer (ESL) which minimizes the excess electron's grand canonical potential and satisfies Poisson's equation.

Within this model the boundary between the plasma sheath and the ESL is given by the distance from the crystallographic interface where the potential for the excess electrons turns from the repulsive sheath potential into the attractive surface potential. This distance is typically on the order of a micron. It gives the position of the effective wall for plasma electrons and ions and thus the portion of the ESL which lays in front of the surface. Most of the surplus electrons trapped in the ESL, that is, the wall charge, will be, however, much closer to the surface or even inside the dielectric depending on the electron affinity.

We presented numerical results for the potential and

the surplus electron distribution at the interface between a helium discharge and the surfaces of MgO, Al<sub>2</sub>O<sub>3</sub>, and SiO<sub>2</sub>, respectively. The electron distribution within the ESL (wall charge) strongly depends on the electron affinity. For negative electron affinity, the conduction band minimum is above the potential just outside the dielectric. Hence, it is energetically unfavorable for electrons to penetrate into the bulk and the surface electrons are bound in the image potential in front of the surface. In this case, their spatial profile changes little over a variation of the surface temperature or the plasma parameters. For positive electron affinity the conduction band minimum is below the potential just outside the dielectric and the surface-bound electrons accumulate inside the wall. The space charge in the bulk broadens if the surface temperature is increased and becomes more peaked if the total surface density of the electrons missing in the sheath is raised through either an increase in the plasma density or the electron temperature. For plasma walls with positive electron affinity the plasma induces also an additional band bending.

Separating the ESL into an interface specific and a space charge region and modeling the bulk of the dielectric as an intrinsic semiconductor we also investigated

how the ESL merges with the bulk of the dielectric. This is particularly important for dielectrics with small energy gaps and positive electron affinities where excess electrons coming from the sheath accumulate not in the image potential in front of the surface but deep inside the wall. In this case the wall charge may also induce a significant band bending.

The ESL should be regarded as the ultimate boundary layer of a bounded gas discharge. Whereas the crude ESL model we proposed neglects the space charge deep inside the bulk of the wall and is thus only applicable to large band gap dielectrics with negative electron affinity where basically the whole wall charge is trapped in the image potential in front of the surface, the refined ESL model keeping the interface specific as well as the space charge region of the ESL provides a quantitative description of the whole spatial structure of the extended charge double-layer which forms at a dielectric plasma wall as a result of the electrons in the ESL and the positive space charge in the plasma sheath.

*Acknowledgments.* This work was supported by the Deutsche Forschungsgemeinschaft (DFG) through the projects B10 and A5 of the transregional collaborative research center SFB/TRR 24.

- 
- <sup>1</sup> O. Ishihara, J. Phys. D: Appl. Phys **40**, R121 (2007).  
<sup>2</sup> V. E. Fortov, A. V. Ivlev, S. A. Khrapak, A. G. Khrapak, and G. E. Morfill, Physics Reports **421**, 1 (2005).  
<sup>3</sup> D. A. Mendis, Plasma Sources Sci. Technol. **11**, A219 (2002).  
<sup>4</sup> U. Kogelschatz, Plasma Chemistry and Plasma Processing **23**, 1 (2003).  
<sup>5</sup> L. Stollenwerk, S. Amiranashvili, J.-P. Boeuf, and H.-G. Purwins, Phys. Rev. Lett. **96**, 255001 (2006).  
<sup>6</sup> L. Stollenwerk, J. G. Laven, and H.-G. Purwins, Phys. Rev. Lett. **98**, 255001 (2007).  
<sup>7</sup> R. Dussart, L. J. Overzet, P. Lefauchaux, T. Dufour, M. Kulsreshath, M. A. Mandra, T. Tillocher, O. Aubry, S. Dozias, P. Ranson, et al., Eur. Phys. J. D **60**, 601 (2010).  
<sup>8</sup> C. J. Wagner, P. A. Tchertchian, and J. G. Eden, Appl. Phys. Lett. **97**, 134102 (2010).  
<sup>9</sup> K. H. Becker, K. H. Schoenbach, and J. G. Eden, J. Phys. D: Appl. Phys **39**, R55 (2006).  
<sup>10</sup> N. P. Ostrom and J. G. Eden, Appl. Phys. Lett. **87**, 141101 (2005).  
<sup>11</sup> M. J. Kushner, J. Phys. D: Appl. Phys **38**, 1633 (2005).  
<sup>12</sup> R. N. Franklin, *Plasma phenomena in gas discharges* (Clarendon Press, Oxford, 1976).  
<sup>13</sup> M. A. Lieberman and A. J. Lichtenberg, *Principles of plasma discharges and materials processing* (Wiley-Interscience, New York, 2005).  
<sup>14</sup> K.-U. Riemann, J. Phys. D: Appl. Phys **24**, 493 (1991).  
<sup>15</sup> K. G. Emeleus and J. R. M. Coulter, Int. J. Electronics **62**, 225 (1987).  
<sup>16</sup> K. G. Emeleus and J. R. M. Coulter, IEE Proceedings **135**, 76 (1988).  
<sup>17</sup> J. F. Behnke, T. Bindemann, H. Deutsch, and K. Becker, Contrib. Plasma Phys. **37**, 345 (1997).  
<sup>18</sup> D. Uhrlandt, M. Schmidt, J. F. Behnke, and T. Bindemann, J. Phys. D: Appl. Phys **33**, 2475 (2000).  
<sup>19</sup> Y. B. Golubovskii, V. A. Maiorov, J. Behnke, and J. F. Behnke, J. Phys. D: Appl. Phys **35**, 751 (2002).  
<sup>20</sup> F. X. Bronold, H. Deutsch, and H. Fehske, Eur. Phys. J. D **54**, 519 (2009).  
<sup>21</sup> R. L. Heinisch, F. X. Bronold, and H. Fehske, Phys. Rev. B **81**, 155420 (2010).  
<sup>22</sup> R. L. Heinisch, F. X. Bronold, and H. Fehske, Phys. Rev. B **82**, 125408 (2010).  
<sup>23</sup> F. X. Bronold, R. L. Heinisch, J. Marbach, and H. Fehske, IEEE Transactions on Plasma Science **39**, 644 (2011).  
<sup>24</sup> R. L. Heinisch, F. X. Bronold, and H. Fehske, Phys. Rev. B **83**, 195407 (2011).  
<sup>25</sup> F. X. Bronold, H. Fehske, H. Kersten, and H. Deutsch, Phys. Rev. Lett. **101**, 175002 (2008).  
<sup>26</sup> F. Stern, Phys. Rev. B **17**, 5009 (1978).  
<sup>27</sup> F. Stern and S. D. Sarma, Phys. Rev. B **30**, 840 (1984).  
<sup>28</sup> J. Planelles and J. L. Movilla, Phys. Rev. B **73**, 235350 (2006).  
<sup>29</sup> E. E. Tkharev and A. L. Danilyuk, Vacuum **35**, 183 (1985).  
<sup>30</sup> N. D. Mermin, Phys. Rev. **137A**, 1441 (1965).  
<sup>31</sup> W. Kohn and L. J. Sham, Phys. Rev. **140A**, 1133 (1965).  
<sup>32</sup> R. T. Tung, Material Science and Engineering **R35**, 1 (2001).  
<sup>33</sup> B. Baumeier, P. Krueger, and J. Pollmann, Phys. Rev. B **76**, 205404 (2007).  
<sup>34</sup> D. Cahen and A. Kahn, Advanced Materials **15**, 271 (2003).  
<sup>35</sup> J. D. Jackson, *Classical electrodynamics* (Wiley, New York, 1998).  
<sup>36</sup> N. W. Ashcroft and N. D. Mermin, *Solid state physics* (Saunders College Publ. Philadelphia, 1976).

<sup>37</sup> H. Lüth, *Solid Surfaces, Interfaces and Thin Films* (Springer Verlag, Berlin, 1992).